Astron. Astrophys. 275, 549–557 (1993)

ASTRONOMY AND ASTROPHYSICS

Tracing the roots of interstellar mid–infrared emission

P. Jenniskens[1,2] **and F.-X. Désert**[1,3,4]

[1] Laboratory Astrophysics Leiden, P.O. Box 9513, NL-2300 RA Leiden, The Netherlands
[2] Sterrewacht Leiden, P.O. Box 9513, NL-2300 RA Leiden, The Netherlands
[3] DEMIRM, Observatoire de Meudon, F-92195 Meudon Cedex, France
[4] Institut d'Astrophysique Spatiale, Bat 121, Université Paris XI, F-91405 Orsay Cedex, France

Received September 23, 1992; accepted March 2, 1993

Abstract. An attempt is made to link components of the interstellar extinction curve to mid infrared emission of interstellar dust. The IRAS mid-infrared emission has been sought for in the direction to all early type stars for which IUE extinction curves have been published. In 44 lines of sight we were able to obtain well defined colours. By comparing the extinction curve components with these IRAS colours, we find that the bump in the extinction curve at 0.218 μm, and not the linear rise or FUV non-linear rise, is systematically weakened in lines of sight where the mid-infrared (12 micron) emitters have been removed.

Key words: dust, extinction – infrared: interstellar: continuum – ultraviolet: interstellar – dust models

1. Introduction

In 1983 the Infrared Astronomical Satellite (IRAS) observed ubiquitous *mid-infrared emission* ($\lambda < 80\mu$m) from the interstellar medium. The emission is at too short a wavelength to be from grains in thermal equilibrium with the ambient radiation field and is thought to be due to very small grains or big molecules, which show temperature fluctuations after absorbing single UV photons (Sellgren 1981, 1984). Two (groups of) non-thermal emitters can be discriminated from correlation studies of the four IRAS pass bands: those emitting at 12 and 25 micron and those emitting at 25, 60 (and 100) micron (e.g. Désert et al. 1990). Because as much as 35% of the total energy emitted in the infrared by diffuse medium dust is from such non-thermal processes (Boulanger & Perault 1988), the absorbers must have a clear signature in the interstellar extinction curve. Establishing a link between emission and extinction properties of dust will put strong constraints on the current dust models.

Many extinction curves have been published from data of the International Ultraviolet Explorer (IUE), operational since 1978. By comparing the flux of reddened and non-reddened early type stars, the wavelength dependence of absorption and scattering of the interstellar matter is derived. Any of the features of the IUE extinction curves, which cover the range $0.32 < \lambda < 0.12\,\mu$m, could be the roots of the mid-infrared emission, because at these wavelengths the extinction of the big classical grains saturates. We follow Fitzpatrick & Massa (1988) in their discrimination of extinction curve components: the bump at 0.218μm, the linear rise and the FUV non-linear rise.

Several recent papers address the connection between the emission and extinction data. They either start from theoretical dust models trying to predict which properties should go together (Chlewicki & Laureijs 1988; Williams 1989; Léger et al. 1989; Désert et al. 1990). Or they search for observational correlations which may contain clues to such a theory (Cox & Leene 1987; Leene & Cox 1987; Hackwell et al. 1991). We shall review these papers along with our own findings in the concluding section.

The research reported in the present paper is based on observations. Compared to previous studies this paper includes an extended set of extinction curves, covering nearly all IUE extinction curves present in the literature. IRAS infrared colours are determined from pixel to pixel scatter diagrams of infrared emission enhancements in the line of sight instead of using an uncertain zodiacal light model to determine the background level.

The paper is organized as follows. Section 2 defines what emission and extinction parameters are to be compared. The reduction procedures are outlined, with emphasis on the IRAS infrared data. The sample of lines of sight is specified in Sect. 3. The infrared data are presented in Sect. 4 with evidence of abundance variations. In Sect. 5 the data are correlated and the results, which indicate that the mid-infrared emission has roots in the bump, possibly in the FUV non-linear rise, but not in the linear rise, are discussed in Sect. 6.

2. Procedure

The infrared emission of a grain in an isotropic interstellar radiation field (J_o) is determined by the balance between the rates

Send offprint requests to: P. Jenniskens, NASA/Ames Research Center, Mail Stop 239-4, Moffett Field, CA 94035-1000, USA.

at which energy is absorbed and emitted (Van de Hulst 1949):

$$\int_{UV} 4\pi C_{abs}(\lambda,a)J_o(\lambda)d\lambda = \int_{IR} 4\pi C_{abs}(\lambda',a,T_{gr})B_{\lambda'}(T_{gr})d\lambda' \quad (1)$$

where Kirchhoff's Law links absorption and emission of one dust component: the material's emissivity at a given wavelength and temperature equals its absorptivity: C_{abs} is the cross–section for absorption per unit mass and B the blackbody emission intensity.

For very small grains or big molecules the total heat capacity is so low that significant temperature fluctuations occur by the absorption of a single UV photon. But because there is enough time between two photon emissions to redistribute energy between the available vibrational levels (Léger & d'Hendecourt 1987), the infrared emission is described as a sum over the grain vibrational temperature distribution.

With N the mass column density of an assembly of carriers of one emission compound, we have for emission:

$$I(\lambda) = B_\lambda(T)(1 - e^{-NC^\lambda_{abs}}) \sim B_\lambda(T)NC^\lambda_{abs} \quad (2)$$

because the infrared emission is usually optically thin. For extinction we have:

$$A(\lambda) = -2.5log\frac{I^*}{I^*_o} \sim NC^\lambda_{ext} \sim NC^\lambda_{abs} \quad (3)$$

where the right equality is true if the albedo is zero (see next section). Equations 2 and 3 give the parameters we want to compare. It is immediately obvious that variations in the ambient radiation field, which determines the factor $B_\lambda(T)$, will cause a scatter in the infrared emission data (e.g. Laureijs 1989; Désert et al. 1990). The method also assumes that emission and absorption data result from the same dust grains, which is never the case because emission is observed in a large beam towards the program star and extends beyond the program star while extinction data are measured in a narrow pencil beam and only between us and the program star. Also, the hot emitting dust may be at a different location in the line of sight than the dense (cold) absorbing dust. There is no way to eliminate this uncertainty, although one may try to optimise this condition.

Finally, there are serious limitations in the definition of absorption (A) and emission (I), which are due to the fact that the observed data are from several dust components, the absolute values are hard to measure, and the extinction data include scattering. In the next paragraphs these factors are discussed for extinction and emission data separately.

2.1. Extinction

Extinction is measured as a decrease in brightness of a background star (at a certain wavelength) compared to a standard star. Because the stars are usually not at the same distance, and the distances are not known precisely enough, a differential decrease in brightness is measured and expressed as E(λ-V) = A(λ) - A(V).

The extinction is normalised to E(B-V) in order to take into account the variable amount of interstellar matter in the line of sight. The resulting extinction curve k(x) is traditionally expressed in terms of inverse wavelength ($x = \lambda^{-1}$ in μm^{-1}):

$$k(x) = \frac{E(\lambda - V)}{E(B-V)} = \frac{(m(\lambda) - V) - (m_o(\lambda) - V_o)}{(B-V) - (B-V)_o} \quad (4)$$

where "$_o$" refers to a non-reddened standard star of the same spectral type as the reddened star.

Correlation studies show that at least four components make up the extinction curve (e.g. Fitzpatrick & Massa 1988, 1990; Jenniskens & Greenberg 1993). These are 1) the extinction by big ($\sim$ 0.1μm) grains, which rises in the visual with x and saturates below 0.3μm (3.3 μm^{-1}) , 2) an associated linear rise (in terms of x) which continues until 0.13 μm (8 μm^{-1}), 3) a bump centered at 0.218μm (4.6 μm^{-1}) and 4) a non-linear rise in the FUV. Any IUE extinction curve (3.2 $< x <$ 8.0 μm^{-1}) can be decomposed into (Fitzpatrick & Massa 1990):

$$k(x) = c_1 + c_2x + c_3[\frac{x^2}{(x^2 - x_o^2)^2 + \gamma^2x^2}] + c_4f(x)$$

$$f(x) = 0.5392(x - 5.9)^2 + 0.0564(x - 5.9)^3 \qquad x > 5.9$$

$$f(x) = 0 \qquad x < 5.9 \quad (5)$$

where c_1, c_2, c_3, c_4, x_o, and γ are the parameters determined for each extinction curve which are sufficient to describe it completely.

The examples shown in Fig. 1 (HD48434 and HD38087) illustrate the decomposition procedure and the definition of the UV extinction parameters used in the text. The black dots are the IUE data, while the smooth line through the data is the final fit. The thick dashed curves are the linear rise, bump Drude and FUV non-linear rise components of the fit. The fit is very good and deviates significantly from the data only when a remnant of the CIV stellar line or saturation problems at the edges of the IUE windows are suspected.

As said, a potentially important limitation for applying Eq. 3 is that the extinction data include scattering. The extinction cross section is defined as: $C_{ext} = C_{abs} + C_{sca}$. The albedo ($C_{sca}/C_{ext}$) of each of the dust components may be estimated as follows. Some data are available for the sum of the components (e.g. Witt 1989), which show an albedo minimum at 220nm, which is consistent with a non scattering bump carrier. Also the scattered light of the Merope reflection nebula does not show a bump and FUV non-linear rise implying pure absorption in these features. There is an increase of scattered intensity toward the FUV, thought to be due to a less foreward scattering phase function at short wavelengths, characteristic of particles small compared to the wavelength, which is due to the carriers of the linear rise. If the grains are much smaller than the wavelength, the albedo is small (< 0.2). This is consistent with the albedo measurements of Witt & Lillie (1976), which show the same albedo at 0.15 and 0.3 μm (about 0.6). Most of this albedo should be due to the saturated big grain extinction, which, according to Mie theory, is equal to 0.5 and wavelength

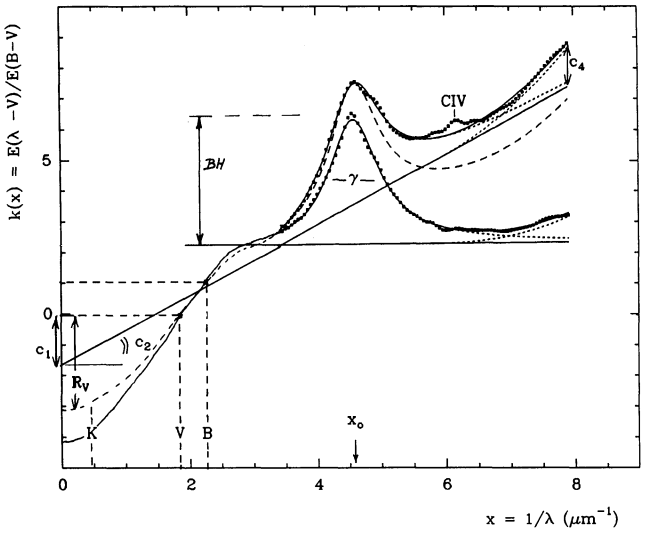

Fig. 1. Extinction curves of HD48434 (upper curve) and HD38087. Black dots are the IUE data. The meaning of the decomposition parameters in Eq. 5 are shown. The FUV non-linear rise component at 8 μm^{-1} equals 2.9 c_4

independent. Therefore, we conclude that the albedo of all dust components is nearly wavelength independent between 0.3 and 0.12μm and that the albedo of the carriers of FUV non-linear rise, bump and linear rise is negligible. Within the observational uncertainties, one can assume: $C_{ext} \sim C_{abs}$ (Eq. 3).

The proportionality factors c_2, c_4 and c_3/γ are proportional to the abundance of the carriers of the linear rise, the FUV non-linear rise and the bump respectively. The bump area is defined as $BA = \frac{\pi c_3}{2\gamma}$. In the correlation studies, we will use the bump height instead (BH):

$$BH = \frac{c_3}{\gamma^2} \tag{6}$$

because it is less sensitive to saturation problems in the short and long wavelength side of the LWR camera, which seem to be indicated by small systematic differences in bump position compared to Fitzpatrick & Massa (1988) (e.g. Jenniskens & Greenberg 1993). Where appropriate, we will give relevant data for both bump height and bump area.

Strictly spoken, the extinction (read: absorption) should be normalised to the extinction of one component, e.g. in terms of A(λ)/A(λ_o) where A(λ_o) refers to a wavelength where only one dust component contributes to the extinction. λ_o can be any wavelength longer than 0.7 μm (Cardelli et al. 1989). At such large wavelengths the shape of the extinction curve is very constant and thought to be due to one (big, a$\sim$ 0.1μm) grain component (Jones & Hyland 1980; Clayton & Mathis 1988; Cardelli et al. 1989; Martin & Whittet 1990). In practice, normalisation to the V passband (0.55μm) will do.

As a matter of fact, the extinction parameters $c_i (i = 1, ..., 4)$ can be transformed to a normalisation in terms of $A(\lambda)/A(V)$ if the ratio of total to selective extinction in the visual (R_V) is known:

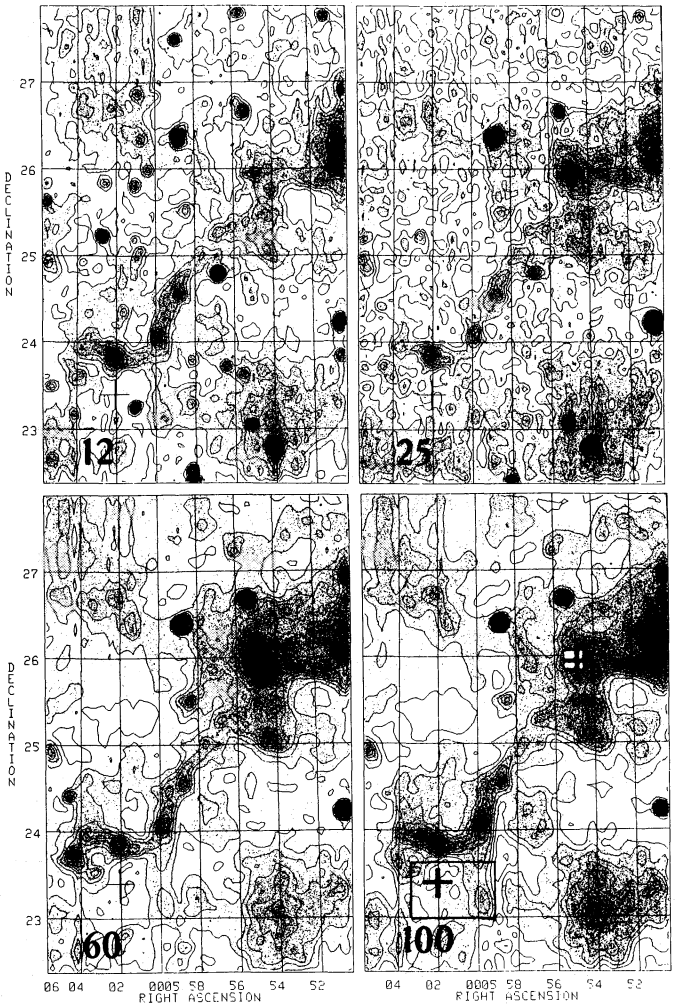

Fig. 2. The four IRAS Skyflux maps that contain the reflection nebula HD40111 (– rejected because of variable colours, upper cross in the 100 μm map) and a diffuse medium line of sight HD251204 (HCON1, plate 53, lower left cross in the 100 μm map). This field is in the ecliptic plane. In spite of the strong zodiacal emission, a consistent background can be chosen in all the maps

$$k(x) = R_V \left(\frac{A(\lambda)}{A(V)} - 1 \right) \tag{7}$$

$$with: \quad R_V = A(V)/E(B-V)$$

R_V is measured from K–band photometry using the empirical relationship (Serkowski et al. 1975):

$$R_V \sim 1.1 \frac{E(V-K)}{E(B-V)} \tag{8}$$

which directly results from the constant shape of the extinction curve for wavelenghts longer than 0.7 μm. From the available K-band photometry in the literature (Aiello et al. 1988), we found a posteriori that the normalisation to A_V did not affect the correlations of emission and extinction significantly. We therefore chose to keep the parameters in the original form in this paper and chose not to include the uncertainties involved by the determination of R_V.

2.2. Emission

The infrared intensity in a given direction is measured as an average over the beam from the observer to a point outside the galaxy. To increase the probability that the extinction and emission are caused by the same dust, one can choose the program stars deliberately at large distance and try to avoid local enhancements of hot dust (Cox & Leene 1987) or one may concentrate on program stars embedded in anomalous dust. The latter assumes that if anomalous emission is seen (i.e. low emission due to an abundance decrease) towards an embedded star with anomalous extinction, the presence of the star is probably related to the origin of the anomaly. For example, in HII regions the 12 micron flux is low relative to 100 micron emission which is linked to an abundance decrease of 12 micron emitters. If an embedded star shows anomalous extinction, then these are probably linked.

This is why we discriminate between diffuse medium lines of sight (DIF) on one hand and diffuse HII regions (BUB), reflection nebulae (REF) and HII regions (HII) on the other. The latter are easily recognized from the IRAS Skyflux maps from their extended (BUB) or local (REF,HII) increased [60/100] colour, while DIF regions have local solar neighbourhood colours which are moreover independent of the projected distance to the star.

For each line of sight, the four IRAS Skyflux plates of either HCON1 or HCON3 (see IRAS Explanatory Supplement, 1985) were reduced using the AIPS software package, according to the following steps.

* A rectangular area of about 3^o by 3^o and containing a line of sight with a known extinction curve was selected.
* A second order polynomial background, dominated by the zodiacal light and by the smooth part of the galactic emission, was removed from the maps. The clipping level above which pixels were excluded for background fitting, was chosen as deep as possible and such as to exclude about the same area in all four maps (Fig. 2). If the zodiacal light dominates the galactic emission at 12 and 25 micron, this is not possible. In that case an initial subtraction of a first order background was applied and a new clipping level was chosen.
* Stripes in the map, due to calibration problems between individual scans and detectors, are removed to a good extent by fitting a linear background through each band of width 2 pixels following the scan direction, through the lowest points in the beginning and ending parts of the band.
* All four maps are processed in this way and convolved with a near circular output beam of 4'x4'.
* Pixel–to–pixel scatter diagrams were made of small areas, 46'x46' for DIF and 23'x23' for BUB/REF/HII lines of sight, that are (approximately) centered on the line of sight for which the UV extinction is measured. Point source contamination is avoided, as much as possible, by choosing the areas appropriately and by estimating the colours [12/100], [25/100] and [60/100] by eye–fit from the scatter diagrams (assuming that the relative errors in the two bands are about the same). The infrared fluxes are not colour corrected.

Removing a second order surface from the map fitted to the lowest levels gives as good a result as subtracting a model of the zodiacal light background (Verter 1987). By choosing a linear background removal for the stripes, we allow for a correction of drifts in detector baseline level. The result was found to be little different from subtracting a constant, but better in the severe cases of strong baseline drift. Usually the cloud features visible at 100 and 60 micron can also be discriminated at 12 and 25 micron (Fig. 2). The colours depend little on the clipping level and polynomial order of the background fitting. We were not able to find a significant effect of the zodiacal light background for those objects that are close to the zodiacal plane.

The normalisation to the 100 micron instensity introduces an uncertainty. The 100 micron emission in diffuse and translucent clouds is proportional to A(V) for a wide range of mid- and far infrared colours (Laureijs et al. 1987; Boulanger et al. 1990). Up to $A_V \sim 2$ magn. (E(B-V)=0.6):

$$I_{100}/A(V) = 16\,\mathrm{MJy\,sr^{-1}\,mag^{-1}} \quad (9)$$

But for dark clouds this ratio can drop by a factor of 2-3 (Boulanger 1989). Our program stars are seen through the clouds, also at short wavelength. They cover $A_V = 1 - 4$ mag. A posteriori we did not recognize an effect of reddening in the infrared colours for stars with $A_V > 2$. For the time being there is no better alternative for normalising the data.

3. Selection criteria

The UV data were selected without prior knowledge of the infrared emission characteristics. The lines of sight that were chosen, are all those for which IUE extinction curves are published in the literature (Aiello et al. 1988; Witt et al. 1984; Seab & Shull 1983; Massa et al. 1983; Clayton & Fitzpatrick 1983; Fitzpatrick & Massa 1988).

Because steep and quickly varying gradients in the galactic background emission make colour determinations difficult in the direction of the galactic center, the sample was restricted to galactic anti–center ($270^o > l > 90^o$) or local lines of sight ($b > 20^o$). Excluded were also the IRAS Point Source Catalogue objects with emission of circumstellar nature ($f_{12} > f_{25}$). Circumstellar dust is known to have different optical properties than ISM dust (see Whittet 1989). The observed circumstellar 12 micron emission may not be due to small grains emitting at a fluctuating temperature, but due to warm large grains close to the star.

All the remaining 103 positions were examined for infrared emission. During the reduction of the infrared data many additional objects have been rejected because no unambiguous colour could be derived. These are lines of sight with only weak enhancements in emission or close to infrared point sources and reflection nebulae where the spatial variations in colours are strong on the scale of the area selected. In the latter case an

Table 1. IRAS uncolourcorrected flux ratio's and IUE extinction curve parameters.

	IR DATA FROM SCATTER PLOTS							err: 2-3 sigma			uv data							positions of iruv sample								
STARNAME	UV	REF.	r14	err	r24	err	r34	err	Q	PS	TYPE	c1	c2	c3	c4	Y	Xo	BH	chisq	RA (1950.0) H M S	DEC o ,	BETA o	D kpc	E(B-V)	R	SP.TYPE	
HD13268	ABC		0.042	0.006	0.044	0.003	0.212	0.002	0	-	dif	-1.14	1.03	2.89	0.38	0.931	4.575	3.33	0.005	02 08 03	55 55	39.9	2.29	0.44	-.-	08 IV	! HD13268
HD13338	WBS		0.043	0.006	0.041	0.006	0.201	0.006	1	-	dif	0.09	0.63	3.35	0.27	0.957	4.605	3.66	0.003	02 08 46	57 42	41.5	1.07	0.53	-.-	B1 V	! HD13338
HD13659	WBS		0.042	0.002	0.053	0.002	0.182	0.004	0	-	dif	-1.15	1.06	2.20	0.63	1.049	4.640	2.00	0.004	02 11 33	56 42	40.4	2.30	0.76	-.-	B1 Ib	! HD13659
HD14442	ABC		0.047	0.005	0.061	0.006	0.216	0.012	0	-	dif	-0.02	0.69	3.63	0.44	0.947	4.590	4.05	0.004	02 18 32	59 19	42.4	2.29	0.73	-.-	O5-6 III	! HD14442
HD16691	ABC		0.030	0.010	0.055	0.005	0.275	0.025	1	Y	dif	-0.20	0.73	3.97	0.48	0.952	4.575	4.38	0.005	02 39 12	56 42	38.8	2.78	0.80	-.-	O5 I	! HD16691
HD34078	WBS		0.095	0.007	0.440	0.060	0.870	0.001	1	Y	ref	0.44	0.57	4.17	0.49	1.105	4.537	3.42	0.005	05 13 00	34 15	11.2	0.46	0.52	3.30	O9.5 Ve	! HD34078
HD36629	ABC		0.059	0.005	0.070	0.010	0.295	0.021	0	-	ref	1.72	0.21	2.84	0.32	0.910	4.576	3.43	0.006	05 30 29	-04 36	-27.8	0.85	0.27	4.15	B2 V	! HD36629
HD37061	ABC		0.030	0.003	0.038	0.003	0.440	0.060	1	Y	HII	1.76	0.02	2.29	0.25	1.055	4.531	2.06	0.008	05 33 04	-05 18	-28.6	0.43	0.52	4.63	B1 V	! HD37061
HD37367	ABC		0.069	0.006	0.084	0.011	0.196	0.009	0	-	dif	0.84	0.53	4.28	0.32	0.936	4.574	4.89	0.004	05 36 08	29 11	5.9	0.35	0.40	-.-	B2 IV-V	! HD37367
HD37674	WBS		0.050	0.006	0.059	0.007	0.370	0.030	1	Y	ref	1.90	0.13	4.21	0.36	0.935	4.610	4.82	0.020	05 37 44	-01 28	-24.8	0.50	0.14	-.-	B3 Vn	! HD37674
HD37903	ABC		0.039	0.002	0.041	0.002	0.323	0.012	0	Y	ref	1.38	0.36	3.72	0.54	1.130	4.607	2.91	0.005	05 39 07	-02 17	-25.6	0.90	0.35	3.96	B1.5 V	! HD37903
HD38087	ABC		0.046	0.007	0.060	0.006	0.256	0.017	0	Y	HII	2.18	0.02	3.65	0.31	0.949	4.568	4.05	0.005	05 40 29	-02 20	-25.7	0.35	0.29	6.36	B5 V	! HD38087
HD38131	ABC		0.081	0.022	0.062	0.005	0.470	0.060	1	Y	ref	-0.50	0.78	4.00	0.37	0.952	4.586	4.41	0.004	05 41 45	35 09	11.8	1.32	0.51	-.-	B1 III	! HD38131
HD47129	ABC		0.051	0.006	0.053	0.006	0.273	0.017	0	-	bub	-1.07	0.95	4.27	0.46	1.052	4.536	3.86	0.004	06 34 43	06 11	-20.4	1.51	0.36	3.68	O7.5-8 III	! HD47129
HD47240	ABC		0.020	0.002	0.023	0.004	0.392	0.014	1	-	bub	0.04	0.79	2.87	0.44	0.863	4.569	3.85	0.005	06 35 13	05 00	-18.2	1.51	0.33	2.99	B1 Ib	! HD47240
HD48099	SS		0.054	0.009	0.073	0.010	0.350	0.020	0	-	bub	-0.47	0.84	2.79	0.51	0.810	4.535	4.25	0.007	06 39 17	06 24	-16.7	1.28	0.27	3.52	O7 V	! HD48099
HD48279	ABC		0.067	0.005	0.076	0.008	0.221	0.007	1	Y	dif	0.14	0.72	3.46	0.47	0.931	4.585	3.99	0.005	06 40 05	01 46	-21.3	1.82	0.43	4.08	O8-7.5 V	! HD48279
HD48434	ABC		0.067	0.015	0.075	0.013	0.240	0.020	1	-	dif	-1.37	1.10	4.22	0.52	1.051	4.587	3.82	0.007	06 41 00	03 59	-19.1	1.01	0.28	3.22	B0.5 III-II	! HD48434
HD53367	WBS		0.034	0.002	0.037	0.002	0.360	0.030	0	Y	ref	0.29	0.59	3.30	0.39	1.120	4.504	2.63	0.002	07 02 04	-10 23	-32.8	1.28	0.73	4.08	B0 IVe	! HD53367
HD53974	ABC		0.037	0.009	0.074	0.016	0.440	0.030	1	Y	ref	-0.14	0.79	3.57	0.43	0.924	4.606	4.18	0.004	07 04 20	-11 13	-33.6	0.73	0.35	2.88	B0 III	! HD53974
HD61827	ABC		0.068	0.006	0.063	0.006	0.152	0.020	1	-	dif	-0.79	0.87	4.17	0.83	1.059	4.609	3.72	0.005	07 37 54	-32 28	-52.9	4.37	0.69	3.03	B3 Ia	! HD61827
HD73882	ABC		0.008	0.003	0.080	0.009	0.560	0.030	0	-	HII	0.02	0.70	3.34	0.63	1.212	4.554	2.27	0.001	08 37 19	-40 15	-55.9	1.82	0.71	3.42	O8 V	! HD73882
HD147701	ABC		0.046	0.003	0.054	0.003	0.357	0.005	0	-	bub	1.05	0.36	4.21	0.90	1.252	4.618	2.69	0.001	16 21 19	-24 55	-3.4	0.20	0.72	3.91	B5 V	! HD147701
HD147889	ABC		0.050	0.001	0.090	0.009	0.739	0.080	0	-	ref	1.57	0.11	4.91	0.88	1.122	4.613	3.90	0.002	16 22 23	-24 21	-2.8	0.20	1.08	4.10	B2 V	! HD147889
HD154445	ABC		0.052	0.002	0.080	0.003	0.198	0.003	0	-	dif	1.48	0.24	4.91	0.51	1.054	4.567	4.42	0.003	17 02 57	-00 49	21.9	0.34	0.42	2.90	B1.5 V	! HD154445
HD209339	ABC		0.061	0.005	0.063	0.005	0.260	0.020	0	-	ref	-0.30	0.76	4.38	0.24	1.020	4.580	4.21	0.006	21 59 09	62 15	64.8	1.17	0.36	-.-	O9 V	! HD209339
HD216532	ABC		0.036	0.005	0.048	0.008	0.373	0.007	0	-	bub	0.52	0.53	4.47	0.40	1.079	4.583	3.84	0.005	22 50 34	62 11	60.1	0.87	0.86	-.-	O8 V	! HD216532
HD216898	ABC		0.039	0.005	0.036	0.006	0.270	0.030	0	-	bub	0.56	0.53	3.88	0.37	0.980	4.594	4.04	0.001	22 53 44	62 02	59.7	0.87	0.85	2.76	O9 V	! HD216898
HD217061	MS		0.036	0.003	0.062	0.008	0.590	0.050	0	-	ref	0.07	0.64	3.53	0.59	0.986	4.597	3.63	0.001	22 54 45	62 21	59.8	0.87	0.96	-.-	B1 Vn	! HD217061
HD217979	MS		0.055	0.007	0.062	0.007	0.280	0.020	0	-	bub	-0.31	0.78	3.12	0.58	0.937	4.603	3.55	0.001	23 01 23	63 17	59.9	0.87	0.61	-.-	B2 V	! HD217979
HD236923	ABC		0.048	0.007	0.034	0.006	0.250	0.010	1	-	ref	-0.35	0.77	3.38	0.52	0.915	4.607	4.04	0.001	01 56 28	59 29	43.8	1.88	0.62	-.-	B2.5 III	! HD236923
HD237019	ABC		0.024	0.002	0.068	0.008	0.520	0.010	0	-	bub	0.15	0.68	2.94	0.51	0.901	4.588	3.62	0.002	02 49 35	60 15	41.6	2.19	0.78	-.-	O8.5 V	! HD237019
HD239729	ABC		0.018	0.006	0.071	0.007	0.516	0.025	1	-	HII	0.36	0.65	3.87	0.77	1.129	4.600	3.04	0.001	21 37 54	57 15	63.7	0.83	0.66	3.04	O9 V	! HD239729
HD251204	ABC		0.078	0.006	0.063	0.005	0.218	0.010	0	-	dif	-0.43	0.76	3.48	0.59	0.931	4.594	4.01	0.004	06 02 03	23 24	0.0	3.74	0.78	-.-	B0 III	! HD251204
HD252325	ABC		0.027	0.003	0.056	0.004	0.510	0.040	0	Y	HII	1.11	0.39	2.70	0.48	0.891	4.612	3.40	0.006	06 06 01	20 39	-2.2	2.59	0.87	3.33	B0-1 V	! HD252325
CAS OB6	ABC		0.034	0.001	0.108	0.017	0.655	0.050	0	-	HII	0.41	0.60	3.54	0.50	0.962	4.590	3.83	0.001	02 29 00	61 12	43.5	2.19	0.80	2.85	(O4 If)	! CASOB6
MON OB2	ABC		0.011	0.001	0.078	0.025	0.670	0.050	0	-	HII	0.19	0.69	3.03	0.58	0.897	4.586	3.77	0.001	06 29 00	05 00	-18.3	1.51	0.49	3.10	(O4 V)	! MONOB2
TR37	CF		0.036	0.008	0.052	0.005	0.335	0.012	1	-	HII	0.12	0.60	4.91	0.38	1.111	4.609	3.98	0.001	21 35 00	57 19	64.1	0.98	0.55	2.77	(B0.5 V)	! TR37
BD+45 973	ABC		0.043	0.009	0.057	0.009	0.200	0.013	0	-	dif	-0.41	0.68	4.38	0.55	1.052	4.565	3.96	0.008	04 39 24	45 32	23.1	0.96	0.72	-.-	B1 V	! BD+45 973
BD+57 2395B	CF		0.043	0.005	0.056	0.004	0.320	0.012	0	-	ref	-0.64	0.99	2.97	0.61	1.030	4.595	2.80	0.015	21 44 36	57 34	63.3	0.98	0.68	2.83	B3 V	! BD+57 2395B
BD+61 2365	MS		0.040	0.005	0.060	0.005	0.530	0.030	0	Y*	bub	0.61	0.44	4.08	0.39	0.943	4.591	4.59	0.001 a)	22 51 21	62 24	60.2	0.87	0.78	-.-	B1 V	! BD+61 2365
BD+62 2125	MS		0.051	0.007	0.055	0.006	0.280	0.020	0	-	bub	-0.08	0.75	3.36	0.43	0.986	4.593	3.46	0.001 a)	22 50 55	63 09	60.7	0.87	0.90	-.-	B1.5 V	! BD+61 2125
BD+63 1964	ABC		0.041	0.004	0.052	0.005	0.297	0.020	1	-	ref	-0.51	0.73	3.29	0.46	0.912	4.612	3.96	0.005	23 15 14	63 51	59.0	1.83	0.95	-.-	B0-0.5 I	! BD+63 1964
HILTNER188	ABC		0.069	0.012	0.064	0.007	0.280	0.030	0	-	dif	-1.51	0.83	2.77	0.47	0.867	4.602	3.69	0.011	01 54 19	59 44	44.1	2.08	0.65	-.-	B2.5 III	! HILTNER 188

a) values by Fitzpatrick and Massa, 1990.

upward bending slope in the band to band scatter diagrams prevents the assignment of a single colour. No information about the UV extinction curve affected these rejection criteria.

All in all only 55 lines of sight resulted in well defined colours. Among these are clusters of stars which represent one line of sight, judging from the small range in UV parameters and the small angular extent of the cluster on the sky. No independent infrared colours of the cluster members could be derived and they are regarded as one line of sight: 5 stars of MonOB2 (HD46106, HD46149, HD46150, HD46202 and HD46223), 6 stars of CasOB6 (HD15558, HD15570, HD15629, BD+60 501 and BD+60 513) and 3 stars of Trumpler37 (HD 205794, HD239710 and HD205948).

This leaves 44 independent lines of sight for our study.

4. Results

4.1. Abundance variations in heated regions

The resulting infrared colours and UV extinction parameters for all available lines of sight are given in Table 1. The error estimate for the infrared data was estimated by eye from the scatter diagrams and is 2–3 σ according to a least squares analysis of some of the graphs. The uncertainties in the extinction curve decomposition parameters have been estimated by Fitzpatrick & Massa (1988) and Jenniskens & Greenberg (1993), and scale with E(B-V).

The diffuse medium values are similar to those given by Boulanger & Perault (1988), but differ from those of Cox & Leene (1987). We assume that the difference is due to an overcorrection of zodiacal light in the data of Cox & Leene. This warrants our attempt to improve the infrared colours by a different background subtraction.

Figure 3 shows the behaviour of [12/100] and [25/100] with a changing [60/100]. Large values of [60/100] are due to variations in the local radiation field energy density (E) and spectrum. The expected behaviour for a variation in E of the diffuse medium (Mathis et al. 1983) without a change of spectrum is shown by a dashed line for a range of values between 0.1x and 10x the normal value of 0.83 eV/cm^3 (from upper point to lower right point). A variation of E accompanied by a change in the spectrum due to the mixing in of emission from a nearby O5 (400 eV/cm^3 at 1pc; upper curve) or B3 (210 eV/cm^3 at 0.15pc; lower curve) are given by full drawn lines. The lines cover distances from 5 pc and further from an O5 star and from 1.5pc and further from a B3 star. These cover the range of radiation fields encountered in this study. We do not consider dust less than 1.5pc from a B3 type star. The black points should follow the O5 line (upper curve) of Fig. 3, which they do not. This conclusion does not change when the 12 micron emission is associated with the bump instead of with the FUV non-linear rise as in the model of Désert et al. (1990). The O5 curve would be slightly displaced but show the general behaviour.

The unusual low 12 micron emission in heated regions was noticed by Boulanger et al. (1988) for different positions in an individual HII region associated with ξPer and was interpreted as strong evidence for abundance variations of the mid infrared emitters. In HII regions the mid infrared emitters are

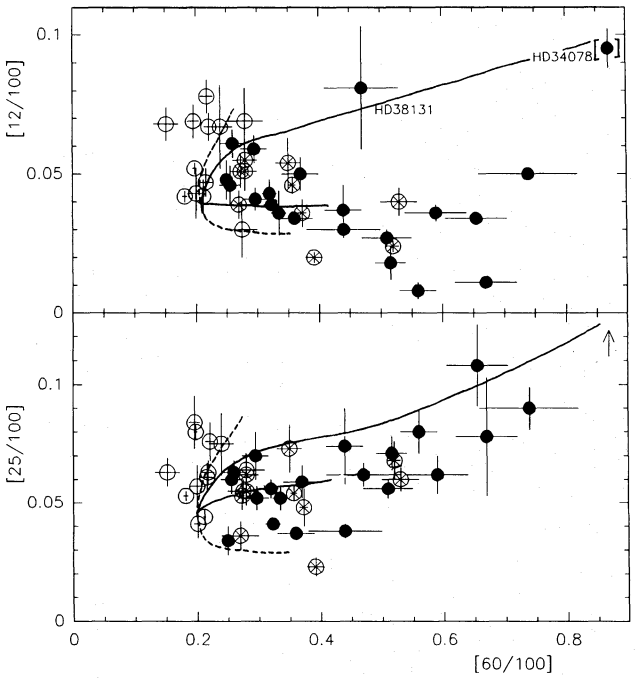

Fig. 3. Interrelationships between the uncolourcorrected flux ratio's from our sample. Different symbols indicate lines of sight with local heating (•), in extended areas of heating (⊗) and in the diffuse medium (◯). Dashed lines indicate a variation of the total interstellar radiation field between 0.1 and 10 times normal. Full drawn lines show the effect of mixing in emission from a B3 and an O5 (upper curve) stellar spectrum for distances from the star larger than 1.5 pc (B3) and larger than 5pc (O5) (from: Désert et al. 1990)

removed, and probably destroyed. A large optical depth will also decrease [12/100] (Désert et al. 1990), but the expected decrease of [12/100] with E(B-V) is not observed.

Two exceptional cases are encountered in Fig. 3. The big grains contribute significantly to the 25 (and 12) micron band toward the star HD34078. The dust must be unusually close to the star. The star is not considered in the following correlation studies. The line of sight to the star HD38131 is the only one which contains a [12/100] colour significantly larger than [25/100]. Note that the star does follow the trend expected for an increased radiation field. The timescale for destruction may exceed the period of time that the dust has been close to this object.

4.2. Abundance variations in the diffuse medium

In addition to the abundance variations in HII regions, strong abundance variations have been reported for diffuse medium lines of sight. Strong variations in [12/100] are observed for nearby clouds that are far away from possible sources of heating (Boulanger et al. 1990). Our data (open points) seem to follow the dashed line closely, indicating a range in radiation field energy density. There is no indication of abundance variations.

Table 2. Correlation coefficients of emission and extinction parameters of Fig. 4. N=43. Between brackets similar values from the data of Leene & Cox (1987) are given. N= 26.

all data	[12/100]	[25/100]	[60/100]
c_2	+0.14	–0.06	–0.29 (–0.51)
BH	+0.40	+0.25	–0.11 (**–0.71**)
c_4	–0.09	+0.29	+0.26 (–0.36)

Table 3a. As Fig. 2. Reflection nebulae and compact HII regions only. N = 20.

REF,HII	[12/100]	[25/100]	[60/100]
c_2	–0.07	+0.04	–0.03
BH	**+0.52**	+0.25	–0.02
c_4	–0.40	+0.40	**+0.62**

Table 3b. As Fig. 3a. Diffuse medium lines of sight only. N=13

DIF	[12/100]	[25/100]	[60/100]
c_2	+0.02	–0.39	+0.10
BH	+0.25	**+0.56**	+0.27
c_4	+0.25	+0.10	–0.36

4.3. The interrelationships

We now consider the interrelationships of extinction and emission data, both in HII regions and in diffuse medium lines of sight (Table 3, Fig. 4). Data from the literature are given in Table 2 (Leene & Cox 1987) and Table 4 (Cox & Leene 1987; Hackwell et al. 1991).

4.3.1. In heated regions

The decrease of [12/100] for heated regions corresponds to a decrease of the bump strength: for BA, the correlation coefficient is r=+0.49, and for BH: r=+0.52 (top left part of Fig. 4). Correlation coefficients are low, because variations in the strength and the spectrum of the radiation field mix in with the sought for variations in abundance of grains. There is no similar systematic decrease for the linear rise or for the FUV non-linear rise (Table 3a).

This link between bump and 12 micron excess, together with the strong decrease of [12/100] with [60/100] in heated areas (Sect. 4.1), should correspond with a decrease of bump strength with increasing [60/100]. This behaviour was found by Leene & Cox (1987). Our data show a similar weak trend (bottom left part of Fig. 4).

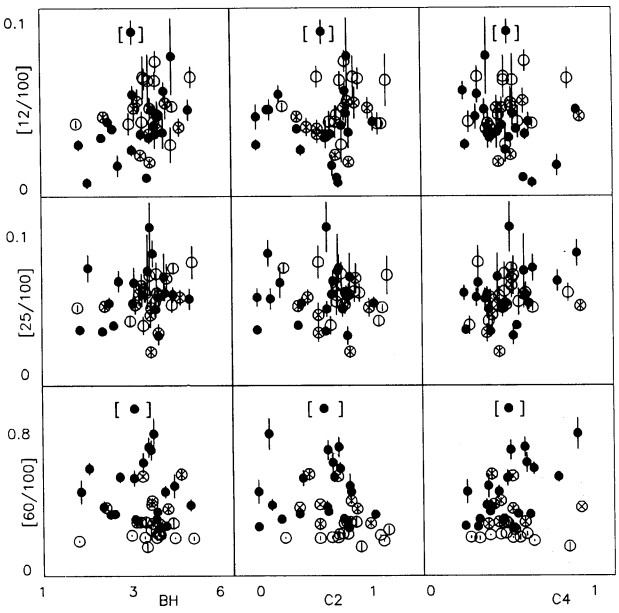

Fig. 4. Diagrams of emission versus extinction parameters. Symbols are as in Fig. 3. The marked point is HD34078, which falls outside the plots containing [25/100]. We note that, if any, there is a positive trend in the top left frame, notably for the dark points (stars in HII regions)

We can not exclude that the carrier of the bump also contributes to 25 and 60 micron emission, because big grain emission adds significantly to these bands in strong radiation fields.

4.3.2. In the diffuse medium

In the diffuse medium (Table 3b) the 25 micron emission correlates weakly with bump strength in our data. But the data are few (N=13) and the result is probably not significant.

Cox & Leene (1987) compared IRAS data with ANS photometry. The stars were chosen to be located at large distances and far away from starforming regions. No correlations were found between bump strength and IRAS colours. We decomposed the ANS photometry into the Fitzpatrick and Massa parameter scheme and, similarly, did not find any trends (Table 4a). Note that the FUV non-linear rise is not well defined by ANS photometric data because the band at shortest wavelength is centered at only 0.155 μm and, furthermore, is affected by CIV mismatches.

The local nature of IRAS cirrus emission poses an uncertainty on the diffuse medium data. Many cirrus clouds are at no more than a few hundred parcecs away (de Vries 1984; de Vries & Le Poole 1985). By choosing stars at larger distance the average extinction curve may be affected by dust that is not seen in the infrared data. Another approach is to take stars that are just a bit further away than the distance where the cirrus emission is found. From such a study, Hackwell et al. (1991) did recently find a correlation (with a negative slope) between the linear rise and [60/100]. However, this correlation is based mainly on the differences in dust properties of two independent lines of sight toward open clusters IC4665 and NGC1647. The measured infrared fluxes, after background subtraction are very low. For reasons of completion, Table 4 lists the correlation coefficients of these data without the stars with $I_{100} < 1$ MJy/sr (N=16), because at such low levels of emission the background subtraction introduces large errors. There may be some other relevant trends in the data: for example, a correlation between bump height and [60/100]. Unfortunately, observational uncertainties in the infrared fluxes add to the scatter introduced by variations in the total interstellar radiation field (Fig. 3), which makes the correlations difficult to interpret.

We conclude from this paragraph that the absence of a strong correlation between bump height and [12/100] in diffuse medium lines of sight is currently not a strong observational argument against the mid infrared emission having roots in the 0.22 μm bump.

Table 4a. Correlation coefficients of emission and extinction parameters of Cox & Leene (1987). IRAS and ANS data. N=53. Diffuse medium lines of sight only. c_4 not well defined. Constant bump width assumed for decomposition.

DIF	[12/100]	[25/100]	[60/100]
c_2	+0.03	+0.01	+0.18
BH	+0.13	+0.09	–0.31
c_4	–0.16	+0.14	–0.06

Table 4b. As Fig. 4a, for data with $I_{100} > 1$ MJy/sterr of Hackwell et al. (1991). N=16. Diffuse medium lines of sight only.

DIF	[12/100]	[25/100]	[60/100]
c_2	–0.03	–0.15	**–0.76**
BH	–0.02	+0.36	**+0.65**
c_4	**–0.65**	+0.06	–0.46

5. Discussion

5.1. Organic grains and big molecules

Because the 12/25 micron emitters should have conspicious roots in the interstellar extinction curve, the weak trend found between bump strength and 12 micron emission for a sample of lines of sight passing HII regions and reflection nebulae, where strong abundance variations are known to be present, is evidence for a generic link between both.

Several authors have proposed such a link. Léger & Puget (1984) and Allamandola et al. (1985) proposed that PAH's are responsible for the UIR bands. Donn (1968) proposed PAH's (Polyaromatic Hydrocarbons, or Platt particles) to be responsible for the shape of the extinction curve in the ultraviolet (bump and part of the linear rise). For the problems that are currently

present in the PAH hypothesis, see Donn et al. (1989). PAH's do show a 'bump' around 0.2μm, but also have a strong NUV absorption and a strong FUV non-linear rise (Léger et al. 1989; Joblin et al. 1992). The latter violates the independent behaviour of FUV non-linear rise and bump. There are possible ways out of the dilemma by considering ionized PAHs and larger than observed PAHs, or smaller than observed amorphous carbon grains, as has been done (e.g. Joblin et al. 1992; Jenniskens et al. 1992).

The bump is traditionally linked to small graphitic grains, possibly partially hydrogenated (Hecht 1986; Perrin & Sivan 1990). Small carbonaceous grains may contribute significant to the mid infrared emission, with an emission band near 7 μm. The constant central position of the bump points toward very small grains $a << 0.01\mu$m. Thus a small grain (3D) scenario comes close to the PAH (2D) hypothesis. Other forms of solid organic materials that have been produced in the laboratory show an absorption band at 0.22μm: the organic residue of photoprocessed organic layers on interstellar dust grains (de Groot et al. 1989) and the stellar outflow products like Quenched Carbonaceous Compounds (Sakata 1989), and also for the theoretical small particles of amorphous carbon (Bussoletti et al. 1987). But the bump like features are too broad, at too long a wavelength, and often contain a steep linear rise.

5.2. The merits of dust models

In a previous study that attempted to link extinction and emission (Désert et al. 1990) it was assumed that there is a relationship between the absorption in the bump of the extinction curve and the 25/60 micron emission, and that the energy absorped in the FUV non-linear rise is responsible for the 12/25 micron emission. We are not able to confirm the link between FUV non-linear rise and the 12/25 micron emission. A way around it is that only part of the PAHs are responsible for the FUV non-linear rise and that the fraction of these PAHs to the total varies from place to place. From that point of view, Jenniskens et al. (1992) found a correlation with H_2 abundance in the line of sight and argued that the FUV non-linear rise could be due to neutral instead of ionised PAHs. In that case, the FUV non-linear rise component also contributes to the mid infrared emission, but the FUV rise is linked to the local strength of the radiation field which affects the temperature of the grains. This may account for the anti-correlation found between FUV non-linear rise and the [12/100] colour (Hackwell et al. 1991, Table 4b).

The models by Chlewicki & Laureijs (1988), using small iron grains, and Williams (1989), using small carbonaceous grains, assume a relationship between the linear rise and the mid infrared excess. The expected correlation between linear rise and mid infrared emission is not found. Instead, there is an anti-correlation with [60/100] (Hackwell et al. 1991), which indicates that the carrier emits in the far infrared. The carrier probably is a small grain ($0.001 < a < 0.01\mu$m). Abundance constraints argue in favour of amorphous carbon grains.

In the dust models that start from an accurate fit of the extinction curve, e.g. Mathis & Whiffen (1989), the authors are vague about the origin of the mid–infrared excess. According to Mathis and Whiffen it may be due to emission of an organic compound that is responsible for the bump and part of the linear rise, or from the cooling of the small grains that are thought to be responsible for the FUV non-linear rise.

If there actually is a link between the mid infrared emission and the bump, the hypothesis of Duley & Williams (1988) and Willams (1989) can be excluded. OH^- absorption in low coordination sites of magnesium silicates is not thought to show the characterstic near infrared emission bands. Other mechanisms based on the mineral component of interstellar dust (Maclean et al. 1982) can be excluded because there is no evidence of silicate emission in the diffuse medium (at 9.7 and 18 μm), which is the fingerprint of very small silicate grains (Désert et al. 1986).

6. Conclusions

A systematic study of infrared emission in the lines of sight of all extinction curves that were published before 1990 has revealed evidence for a link between mid–infrared emission and absorption by bump carriers: a strong abundance decrease of 12 micron emitters in regions with strong UV radiation fields is reflected in a weakening of the bump, not in a weakening of the linear rise or the FUV non–linear rise.

Absorption in the bump may not be the only source of the large amount of infrared emission. Of the other two extinction curve components that are candidate, the FUV non–linear rise is a possible second source. The large variations of FUV non–linear rise compared to two other components of the extinction curve have been linked to a change in a physical state (i.e. ionised versus neutral) instead of abundance. The amount of ionisation will mix up with the abundance variations and increase the scatter in the data.

There is no evidence that this argument applies for the linear rise component, and we conclude that the linear rise in the extinction curve is not related to the mid–infrared emission.

Future work should concentrate on well defined lines of sight, for example local diffuse medium dust, where line of sight problems are as small as possible. The ISO satellite may prove to be a useful tool for measuring infrared emission towards stars for which IUE extinction curves can be measured.

Acknowledgements. We are indebted to S. Aiello, B. Barsella and G. Chlewicki for making available to us the large dataset of UV spectra. The article has benefited from many stimulating discussions with M.S. de Groot, J. M. Greenberg, H.J. Habing, H.C. van der Hulst, R.J. Laureijs, G. Chlewicki and A.G.G.M. Tielens. F.X.D. thanks an ESA Fellowship and thanks Mayo Greenberg and the members of the Laboratory Astrophysics for a pleasant stay in Leiden.

References

Aiello S., Barsella B., Chlewicki G., Mayo Greenberg J., Patriarchi P., Perinotto M., 1988, A& AS 73, 195
Allamandola L.J., Tielens A.G.G.M., Barker J.R., 1985, ApJ 290, L25
Bussoletti E., Colangeli L, Orofino V., 1987, ApJ 321, L87

Boulanger F., Pérault M., 1988, ApJ 330, 964
Boulanger F., Beichman C., Désert F.–X., Helou G., Pérault M., Ryter C., 1988, ApJ 332, 328
Boulanger F., 1989, in *The physics and chemistry of interstellar molecular clouds*, Winnewisser G., Armstrong J.T., eds.
Boulanger F., Falgarone E., Puget J.L, Helou G., 1990, ApJ 364, 136
Cardelli J.A., Clayton G.C., Mathis J.S., 1989, ApJ 345, 245
Chlewicki G., Laureijs R.J., 1988, A& A 207, L11
Clayton G.C., Fitzpatrick E.L., 1987, AJ 93, 157
Clayton G.C., Mathis J.S., 1988, ApJ 327, 911
Cox P., Leene A., 1987, A& A 174, 203
Désert F. X., Boulanger F., Léger A., Puget J.L., Sellgren K., 1986, A& A 159, 328
Désert F. X., Boulanger F., Puget J.L., 1990, A& A 237, 215
Donn B.D., 1968, ApJ 152, L129
Donn B.D., Allen J.E., Khana R.K., 1989, in *Interstellar Dust*, Allamandola and Tielens (eds.), p. 181
Duley W.W., Williams D.A., 1988, MNRAS 231, 969
Fitzpatrick E.L., Massa D., 1988, ApJ 328, 734
Fitzpatrick E.L., Massa D., 1990, ApJS 72, 163
Giard M., Pajot F., Lamarre J.M., Serra G., Caux E., 1989 A& A 215, 92
de Groot M.S., van der Zwet G.P., Jenniskens P., Bauer R., Baas F., Greenberg J.M., 1989 in *Dust in the Universe*, Bailey M.E. and Williams D.A. (eds), 265
Hackwell J., Hecht J.H., Tapia M., 1991, ApJ 375, 163
Hecht J.H., 1986, ApJ 305, 817
van de Hulst, H.C., 1946, Rech. Astron. Obs. Utrecht 11, 1
Jenniskens P., Greenberg J.M., 1993, A& A to be published
Jenniskens P., Ehrenfreund P., Desert F.X., 1992, A& A 265, L1
Joblin C., Léger A., Martin P., 1992, 393, L79
Jones T.L., Hyland A.R., 1980, MNRAS 192, 359
Laureijs R.J., Mattila K., Schnur G., 1987, A& A 184, 269
Laureijs R.J., Chlewicki G., Clark F.O., 1988, A& A 192, L13
Laureijs R.J., 1989, *Infrared Properties of Dust in Interstellar Clouds*, PhD–thesis, RU Groningen
Leene A., Cox P., 1987, A&A 174, L1
Léger A., Puget J.L., 1984, A& A 137, L5
Léger A., d'Hendecourt L., 1987, in *Polycyclic Aromatic Hydrocarbons and Astrophysics*, Léger et al. (eds), 223 1989 in *Interstellar Dust* Tielens and Allamandola (eds.), p. 173
Léger A., Verstraete L., d'Hendrecourt L., Défourneau D., Dutuit O., Schmidt W., Laver J.C., 1989, in *Interstellar Dust*, Allamandola L.J. and Tielens A.G.G.M. (eds.), 103
Maclean S., Duley W.W., Millar T.J., 1982, ApJ 256, L61
Massa D., Savage B.D., Fitzpatrick E.F., 1983, ApJ 266, 662
Martin P.G., Whittet D.C.B., 1990, ApJ 357, 113
Mathis J., Mezger P., Panagia N., 1983, A& A 128, 212
Mathis J.S., Whiffen G., 1989, ApJ 341, 808
Perrin J.M., Sivan J.P., 1990, A& A 228, 238
Sakata A., Wada S., 1989, in *Interstellar Dust*, Allamandola L.J. and Tielens A.G.G.M. (eds.), 191
Seab C.G., Shull J.M., 1983, ApJ 275, 652
Sellgren K., 1981, ApJ 245, 138
Sellgren K., 1984, ApJ 277, 623
Serkowski K., Mathewson D.S., Ford V.L., 1975, ApJ 196, 261
Verter F., 1987, *Techniques for removing zodiacal emission from IRAS SKy Flux Plates* NASA-LEP preprint
de Vries C.P., 1984, "Optical and Infrared Observations of high latitude dust clouds", PhD Thesis, Leiden University
de Vries C.P., Le Poole R.S., 1985, A& A 145, L7
Whittet D.C.B., 1989, in *Interstellar Dust*, Tielens and Allamandola (eds.), 445
Williams D.A., 1989, in *Interstellar Dust*, Tielens and Allamandola (eds.), 367
Witt A.N., Lillie C.F., 1976, A& A 25, 397
Witt A.N., Bohlin R.C., Stecher T.P., 1984, ApJ 279, 689
Witt A.N., 1989, in *Interstellar Dust*, Allamandola L.J. and Tielens A.G.G.M. (eds.), 87

This article was processed by the author using Springer-Verlag TEX A&A macro package 1992.